Determination of the Three-Dimensional Solution Structure of Noxiustoxin: Analysis of Structural Differences with Related Short-Chain Scorpion Toxins[†,‡]

Marc Dauplais,[§] Bernard Gilquin,*[,§] Lourival D. Possani,[||] Georgina Gurrola-Briones,[||] Christian Roumestand,[§,⊥] and André Ménez[§]

Département d'Ingénierie et d'Etude des Protéines, CE-Saclay, 91191 Gif-sur-Yvette Cedex, France, and Departement of Molecular Recognition and Structural Biology, Instituto de Biotecnologia, Univesidad Autonoma de México, Apartado Postal 510-3, Cuernavaca, Morelos 622271, Mexico

Received July 24, 1995; Revised Manuscript Received October 4, 1995[⊗]

ABSTRACT: The 3D structure of noxiustoxin, the first identified scorpion toxin acting on K^+ channels, has been elucidated by NMR and molecular modeling. Thirty-nine solution structures were calculated using 572 distance and 42 dihedral restraints. The average atomic rms deviation between the refined structures and the mean structure is 0.75 Å for the backbone atoms. Noxiustoxin adopts a α/β scaffold constituted of a three-stranded β-sheet (residues 2−3, 25−30, 33−38) linked to a helix (residues 10−20) through two disulfide bridges. A comparison between the 3D structure of noxiustoxin and those of other structurally and functionally related scorpion toxins (charybdotoxin, PO5-NH_2, kaliotoxin) revealed a bending capacity of the helix and a variability in the relative orientations between the helix and the β-sheet. These two features highlight the plasticity of the α/β scaffold and offer a structural explanation for the capacity of the fold to accommodate an additional alanine residue in the Gly-x-Cys pattern of a previously proposed consensus sequence [Bontems et al. (1991) *Science 254*, 1521−1523]. Our structural data also emphasize the possibility that the β-sheet of NTX is implicated in the capacity of NTX to recognize voltage-dependent K^+ channels.

The potassium channels form a large family of proteins expressed at the surface of various eukaryotic cell types, including T-lymphocytes and yeast and liver cells, and are involved in neuromodulation of excitable cells. Permeability of voltage-dependent potassium channels has been known for a long time to be affected by scorpion venoms (Koppenhöfer & Schmidt, 1968; Narahasi et al., 1972; Romey et al., 1975). In 1982, a scorpion toxin affecting potassium channel activity, by depressing peak permeability of K^+ channels of squid giant axons, was isolated (Carbone et al., 1982; Possani et al., 1982). This toxin, called noxiustoxin (NTX),[1] is a polypeptide of 39 residues with three disulfide bridges. It represents 1% of the proteic fraction from the venom of the Mexican scorpion *Centruroides noxius* Hoffmann. Subsequently, it was shown that NTX recognizes the delayed rectifier current channel of squid giant axon (K_D = 390 nM) (Carbone et al., 1982), the voltage-dependent K^+ channels in T-lymphocytes (K_D = 0.2 nM) (Sands et al., 1989), the Ca^{2+}-dependent large conductance K^+ channels of the skeletal muscle (K_D = 450 nM) (Valdivia et al., 1988), and the small conductance K_{Ca} channels from bovine aortic endothelial cells (K_D = 300 nM) (Vaca et al., 1993). Fragments of NTX were tested *in vivo* and on Ca^{2+}-dependent channels (Gurolla et al., 1989; Vaca et al., 1993), revealing that the amino-terminal extremity of NTX was required for both types of activity, the shortest active peptide being composed of residues 1−6. Despite the fact that NTX was the first K^+ channel-acting scorpion toxin to be discovered, its molecular mode of action as well as its tertiary structure remains to be elucidated.

Several other scorpion toxins targeted toward K^+ channels have been isolated during the past decade (Figure 1), and since 1992, the structures of a number of these toxins have been determined by NMR spectroscopy and molecular modeling. These include charybdotoxin (ChTX) (Bontems et al., 1992), iberiotoxin (IbTX) (Johnson & Sugg, 1992), PO5-NH_2 (Meunier et al., 1993), kaliotoxin (KTX) (Fernandez et al., 1994), and margatoxin (MgTX) (Johnson et al., 1994). These toxins share sequence similarities and an analogous fold, characterized by an antiparallel β-sheet linked to a helix by two disulfide bridges. A signature of this fold has been proposed to comprise the six cysteines and one glycine according to the following consensus sequence: Cys-[...]-Cys-x-x-x-Cys-[...]-Gly-x-Cys-[...]-Cys-x-Cys (Bontems et al., 1991). However, despite this structural similarity, the K^+ channel-acting scorpion toxins differ in their biological activities. For instance, two similar toxins, NTX and MgTX which share 79% sequence analogy, both bind to $K_{v1,3}$ channels with a high affinity, but while MgTX is highly

[†] This work was partially supported by DRET (French government) and by Grant 75191-527104 from the Howard Hughes Medical Institute to L.D.P.

[‡] The atomic coordinates of the noxiustoxin structure have been deposited in the Brookhaven Protein Data Bank (file name 1SXM).

* To whom correspondence should be addressed.

[§] CE-Saclay.

[||] Univesidad Autonoma de México.

[⊥] Present address: Centre de Biochimie Structurale, CNRS-UMR 995, INSERM U414, Université de Montpellier, Faculté de Pharmacie, 15 avenue Charles Flahaut, 34 060 Montpellier Cedex 1, France.

[⊗] Abstract published in *Advance ACS Abstracts,* November 15, 1995.

[1] Abbreviations: NTX, noxiustoxin; ChTX, charybdotoxin; IbTX, iberiotoxin; KTX, kaliotoxin; MgTX, margatoxin; NMR, nuclear magnetic resonance; 2D, two dimensional; COSY, correlated spectroscopy; DQF-COSY, double-quantum-filtered correlated spectroscopy; TOCSY, total correlated spectroscopy; NOE, nuclear Overhauser effect; rmsd, root-mean-square deviation; BK, large-conductance Ca^{2+}-activated K^+ channel; SK, small-conductance Ca^{2+}-activated K^+ channel; $K_{v1,3}$, delayed rectifier voltage-dependent K^+ channel; rSA, relative surface accessibility; PDB, protein data bank.

0006-2960/95/0434-16563$09.00/0

		1	2	3	4	5	6	7	8	9	10	11	12	13	14	15	16	17	18	19	20	21	22	23	24	25	26	27	28	29	30	31	32	33	34	35	36	37	38	39	Similarity
		-	b	b	b	-	-	e	e	-	a	a	a	a	a	a	a	a	a	a	a	-	-	-	-	b	b	b	b	b	b	-	-	b	b	b	b	b	b	-	
NTX	39	T	I	I	N	V	K	C	T	S	P	K	Q	C	S	K	P	C	K	E	L	Y	G	S	S	A	G	A	K	C	M	N	G	K	C	K	C	Y	N	N	100%
MgTX	39	T	I	I	N	V	K	C	T	S	P	K	Q	C	L	P	P	C	K	A	Q	F	G	Q	S	A	G	A	K	C	M	N	G	K	C	K	C	Y	P	H	79%
ChTX	37	Z	F	T	N	V	S	C	T	T	S	K	E	C	W	S	V	C	Q	R	L	H	N	T	S	-	R	G	K	C	M	N	K	K	C	R	C	Y	S		44%
IbTX	37	Z	F	T	D	V	D	C	S	V	S	K	E	C	W	S	V	C	K	D	L	F	G	V	D	-	R	G	K	C	M	G	K	K	C	R	C	Y	Q		38%
KTX	37	G	V	E	I	N	V	K	C	S	G	S	P	Q	C	L	K	P	C	K	D	A	G	M	R	-	-	F	G	K	C	M	N	R	K	C	H	C	T	P		46%
PO5-NH2	31				T	-	V	-	C	N		L	R	R	C	Q	L	S	C	R	S	L	G	-	-	L	-	L	G	K	C	I	G	V	K	C	E	C	V	K	H	23%

FIGURE 1: Sequences of some scorpion toxins with the same disulfide pattern as NTX. The percentage of similarity to NTX is indicated.

specific for this channel (Garcia-Calvo et al., 1993; Leonard et al., 1992), NTX also binds to BK. Conversely, two less homologous proteins, NTX and ChTX (46% homology), both bind to the BK and $K_{v1,3}$ channels (Miller et al., 1985; Swanson et al., 1990) but with reversed affinities, ChTX diplaying a higher affinity for BK and NTX for $K_{v1,3}$. The mechanism associated with binding to K^+ channel proteins was investigated for some of these toxins. ChTX was proposed to bind the high-conductance Ca^{2+}-activated K^+ channel in an outer vestibule near the conduction pore (Park et al., 1992). In this model, ChTX occludes the entry of the pore and the Lys27 residue enters the pore. An identical mechanism was proposed to account for the binding of IbTX to BK channels (Giangiacomo et al., 1992) and for the binding of ChTX to the voltage-gated type A Shaker channel (Goldstein et al., 1993). Clearly, the α/β fold adopted by the scorpion toxins is capable of exerting a great body of functional variability, presumably reflecting, at least to some extent, the diversity of K^+ channels; however, the detailed structural basis for this variability is still poorly understood.

Therefore, we decided to investigate the three-dimensional structure of NTX, at the highest possible resolution, not only to better understand the mode of action of this toxin but also to clarify its functional differences with respect to other K^+ channel-acting toxins. In this respect, it should be noted that NTX exhibits two major sequential differences when compared to most other K^+ channel-acting toxins from scorpion venoms. First, it includes two prolines in a region that adopts a helical organization in related toxins. Second, the Gly-x-Cys pattern of the consensus sequence comprises an additional alanine residue in NTX, at position $i-2$ to the cysteine, although it was claimed that a glycine was required at this position due to the lack of local space in the contact area of the helix and the β-sheet (Bontems et al., 1991). MgTX also possesses these features; however, no definite explanation emerged from previous structural studies as to how the fold accommodates them (Johnson et al., 1994). We, therefore, report on the 3D structure of natural NTX, isolated from the scorpion *C. noxius* Hoffmann and determined by NMR spectroscopy and molecular modeling. On the basis of these new data, a comparative structural analysis with other functionally related scorpion toxins indicates that there is a remarkable plasticity within the α/β scaffold and hence that the two features mentioned above may be linked.

MATERIALS AND METHODS

Sample Preparation. The noxiustoxin was purified according to a method already described (Possani et al., 1982). Five milligrams of noxiustoxin was dissolved in 0.4 mL of solvent, leading to a final concentration of 3 mM. The solvents were either H_2O (5% D_2O for the lock) or D_2O after complete exchange of all labile protons. The pH was 3.5, and chemical shifts were measured relative to TSP-d_4.

NMR Experiments. All but exchange NMR experiments were performed at 600 MHz (AMX600 Brüker spectrometer) at two temperatures, 20 and 30 °C, in order to solve assignment ambiguities. At each temperature and for each solvent, a COSY spectrum (Aue et al., 1976) (DQF-COSY in D_2O; Rance et al., 1983), a NOESY spectrum (300 ms mixing time) (Kumar et al., 1980), and a TOCSY spectrum (Braunschweiler & Ernst, 1983; Davis & Bax, 1985) were recorded for complete assignment. TOCSY spectra were recorded with an 80 ms isotropic mixing time using a WALTZ-16 composite sequence (Shaka et al., 1983) and a pair of Z-filter pulses with a delay of 3 ms on either end of the mixing time to overcome phase anomalies (Rance, 1987). At 20 °C, a NOESY spectrum was recorded for each solvent with a 150 ms mixing time for peak integration. Quadrature detection was performed using the States method (States et al., 1986) in the indirect dimension and using simultaneous mode acquisition in the directly detected dimension. The water signal was suppressed by low-power irradiation at all times except during t_1 and t_2. The spectra were recorded with 256 (t_1) × 1024 (t_2) complex data points, except for DQF-COSY [512 (t_1) × 2048 (t_2)], and with a sweep width of 7812.5 Hz (6666.7 Hz for experiments in D_2O). All data were processed either on an X32 Brüker using UXNMR software or on a Sun Sparc Station using FELIX software (Biosym Technologies, San Diego). Prior to Fourier transformation, the spectra were weighted with a shifted sine-bell window function and were zero-filled in the t_1 dimension to yield 1K × 1K matrices after reduction (1K × 4K for the DQF-COSY). Base plane distortions were corrected using a third-order polynomial function in both dimensions.

The $^3J_{NH-H\alpha}$ (respectively $^3J_{H\alpha-H\beta}$) coupling constants were measured from the high-resolution COSY (respectively DQF-COSY) spectra with a 1.9 Hz digital resolution in the ω_2 axis (1.6 in D_2O).

Proton−deuterium exchange of the amide protons was recorded at 500 MHz (AMX500 Brüker spectrometer). The relative rates of NH proton exchange were determined by qualitatively following the kinetics of proton−deuterium exchange. Three 2.5 h TOCSY spectra (30 ms mixing time) were recorded. The first one was recorded at 10 °C, immediately after dissolution in D_2O of a freshly lyophilized sample of NTX. After having recorded the first experiment, the temperature was increased to 20 °C and the sample equilibrated for 1 h. The second TOCSY was then started. Accordingly, the third TOCSY was recorded after an equilibration at 30 °C for 1 h, following the end of the second experiment.

Experimental Restraints. Each NOE was integrated using FELIX software (Biosym Technologies, San Diego), and the NOE intensity was converted into an interproton distance using the relationship:

$$d_{ij} = d_{ref}/(I_{ij}/I_{ref})^{1/6}$$

where the reference intensity (I_{ref}) refers to the NOE cross peak between the Hδ and Hϵ protons of Tyr21. A 2.48 Å

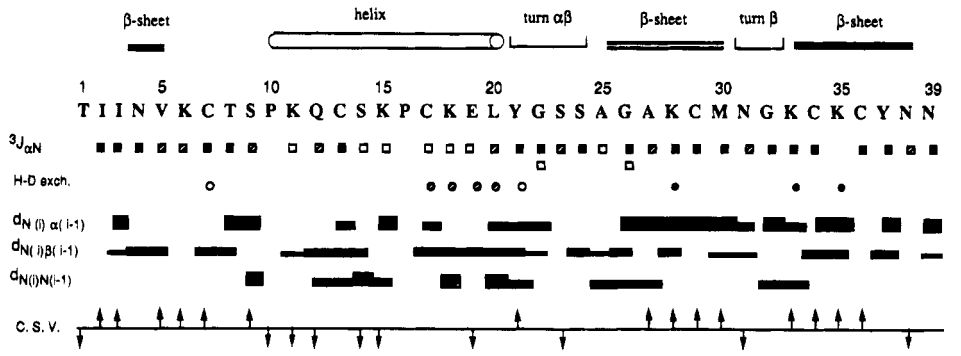

FIGURE 2: NMR data used for the sequence-specific assignment and the secondary structure identification. The data are compiled from NOESY and COSY spectra at 20 °C (pH 3.5). Exchange data come from three TOCSY spectra, recorded respectively at 10 °C after 5 min, at 20 °C after 3 h, and at 30 °C after 7 h. $^3J_{\alpha N}$: (□) $^3J_{\alpha N} \leq 6$ Hz; (◪) 6 Hz $\leq {}^3J_{\alpha N} \leq 9$ Hz; (■) $^3J_{\alpha N} \geq 9$ Hz. H−D exchange experiments: amido proton signal still present in TOCSY spectra recorded at: (○) 10 °C, (◑) 20 °C, and (●) 30 °C. C. S. I. (chemical shift index): according to the Wishart method (Wishart et al., 1992). A chemical shift variation larger than 0.1 from the average value of the α-proton for the concerned residue is represented by an arrow, directed upward for a positive difference and downward for a negative difference.

distance between these protons was used for calibration. All I_{ij} NOE intensities come from the 20 °C, 150 ms mixing time NOESY spectra. A range of ±25% of the distance value was used to define the upper and lower bounds of the restraints. For protons which could not be stereospecifically assigned, the lower bound was fixed to the sum of the hydrogen van der Waals radii (2 × 0.9 Å = 1.8 Å). A total of 572 upper and lower distance restraints (262 intraresidues, 116 sequential, 53 short-range ($|i - j| \leq 4$), and 106 long-range ($|i - j| > 4$) restraints, and 35 ambiguous restraints) were derived from NOE spectra, yielding an average number of 14 restraints per residue.

A total of 24 dihedral ϕ angle restraints were obtained from the $^3J_{NH-H\alpha}$ coupling constants (Figure 2) using the Karplus relation (Karplus, 1963) with the Pardi coefficients (Pardi et al., 1984). Eighteen χ_1 angle restraints were derived from the analysis of $^3J_{H\alpha-H\beta}$ coupling constants and intraresidue NOEs (Hyberts et al., 1987). The boundaries of intervals were fixed to ±45°.

Hydrogen Bonds. In the H−D exchange experiments, nine amide protons showed slow exchange kinetics. Three of them (Lys28 NH, Lys33 NH, and Lys35 NH) displayed a persistent signal and were observed in the last TOCSY, recorded 7 h after the dissolution of the toxin in D_2O (Figure 2). Since these three protons were located in a part of the toxin identified as a β-sheet, the acceptors of the hydrogen bonds could be easily deduced from cross-strand NOE connectivities. Only these three hydrogen bonds, between Lys28 NH and Lys35 O, Lys33 NH and Met30 O, and Lys35 NH and Lys28 O, were introduced in DIANA and simulated annealing calculations. For each hydrogen bond, two restraints were used: 1.7−2.0 Å between the hydrogen and its oxygen acceptor and 2.7−3.0 Å between the nitrogen atom of the donor and the oxygen acceptor atom (Baker & Hubbard, 1984).

A hydrogen bond analysis was done after simulated annealing in order to identify the acceptors for the hydrogen bonds of the four amide protons located in the helix and showing slow exchange kinetics (amide protons of the Cys17, Lys18, Glu19, and Leu20 residues). After simulated annealing, $i,i+4$ hydrogen bonds were found for them in 100%, 90%, 90%, and 92% of the 49 calculated structures, respectively. Consequently, four extra restraints were introduced in the last restrained minimization step, setting a 2.60 Å distance between the amide proton and its hydrogen acceptor. It was also noted that, in the structures derived from simulated annealing, the amide protons of Gln12, Cys13, and Ser14 were always committed in $i,i+3$ hydrogen bonding, but since slow exchange was not observed for these protons, no restraint was introduced.

The complete list of experimental restraints is available upon request from the authors.

3D Structure Calculation. 3D structures were deduced from the experimental distance and angle restraints using distance geometry and simulated annealing calculations.

Distance geometry calculations were performed using the variable target function program DIANA (Güntert et al., 1991). Additional distance restraints were included in the DIANA software to define the three disulfide bridges, composed of an upper and lower boundary of 2.0 and 2.1 Å for $d(S^\gamma,S^\gamma)$, respectively, and 3.0 and 3.1 Å for $d(C^\beta,S^\gamma)$, respectively. Preliminary structures were used for solving ambiguities or correcting assignments; then a set of 100 structures was generated with the final list of restraints.

Among the last 100 structures generated by DIANA, 40 structures presented a target function lower than 2.5 with no distance violations greater than 0.65 Å, and 54 had a function smaller than 10 and no violations greater than 1 Å. The ϕ and χ_1 angle maximum violation was 5°. Considering the high number of constraints (14 per residue) and the low value of the target function, the NMR data appear to be consistent, and the 50 structures with the lower target function value were further refined by simulated annealing calculations using X-PLOR (Brünger et al., 1987; Brünger, 1992).

The simulated annealing protocol employed was derived from the one described previously (Gippert et al., 1990) and implemented in our laboratory (Zinn-Justin et al., 1992; Gilquin et al., 1993; Segalas et al., 1995). The target function was similar to that used by Nilges et al. (1988). A force field adapted for NMR structure determination (files parallhdg.pro and topallhdg.pro in X-PLOR 3.1) was used. A last dynamic at 600 K and a restrained minimization were carried out using the force field derived from CHARMM22 in order to perform a final optimization of the structure. The structure was displayed and analyzed on a Silicon D_Graphics 4D/25 station using the SYBYL package (Tripos Associate Inc.)

Among the 50 structures derived from DIANA and simulated annealing, one always kept a high-energy value and was eliminated. The 49 remaining ones were refined

with the CHARMM22 force field. All the refined structures present no violation larger than 0.4 Å. The 39 structures with lower energy were kept for further analysis and statistics. None of them has any violation larger than 0.3 Å.

P-Curve Geometry Analysis. The geometry analysis of the structures was done with P-Curve software (Sklenar et al., 1989; Furois-Corbin et al., 1994). The aim of this software is to enable calculation of the helicoidal structure of a protein starting from the atomic coordinates of its peptide backbone. The software algorithm yields a unique curved axis and a full set of helicoidal parameters describing the location of each peptide unit. For residues located in the helix, the curved axis approximates the helix axis; for residues in a β-strand, the axis is a straight line through all the residues of the strand. For each residue, an unitary vector of the local curved axis is assessed. This software yields then a local description of the secondary structure and enables then a comparison of fine homologous structures. With the help of the curved axis unitary vectors of the residues located in the helix and β-sheet, a calculation of the bend angle of the helix and of the angle between the helix axis and β-sheet can be performed.

As the determination of the extremity of the helix is often controversial, we did not take into account the first and the last residue of the helix when evaluating the curvature. In order to decrease single-residue artifacts, an average of the four angles existing between the unitary vectors of the second and the third residues of one extremity of the helix with those of the other extremity was calculated. The angle between the helix and the β-sheet was assessed by averaging angles between unitary vectors of the two central residues of the helix (three if helix length is odd) with unitary vectors of the first two residues located on the central strand of the β-sheet. The accuracy of the angle value was estimated to be approximately 7°.

DELPHI Software. The DELPHI program (Gilson & Honig, 1988) solves the linearized Poisson−Boltzmann equation at the nodes of a cubic lattice. The parameters used were 2.0 for the dielectric constant of the protein, 80.0 for the dielectric constant of the solvent, 0 M for the ionic strength, 0 Å for the exclusion radius of ions, and 1.4 Å for the exclusion radius of the solvent. The calculated electrostatic potential surfaces were displayed and graphically analyzed with INSIGHT software (Biosym Technologies, San Diego).

RESULTS

Resonance Assignment. The sequence-specific assignment of NTX was achieved according to the standard method developed by Wüthrich (1986). Selected spectra recorded at two temperatures allowed resolution of ambiguities due to overlapping resonance signals. Sequential connectivities were obtained from NOESY spectra recorded with a 300 ms mixing time in H_2O. Several reliable starting points were used for the toxin assignment: the single valine (Val5) and the isoleucines (Ile2−Ile3) for the N-terminal extremity of the toxin, the duet Leu20-Tyr21 (unique leucine) for the end of the helix, the triplet Ala25-Gly26-Ala27 (including the only two alanines) for the beginning of the β-sheet, and Tyr37 for the C-terminal region. Figure 3 shows the sequential assigment for the β-sheet (Ala25−Asn39). The

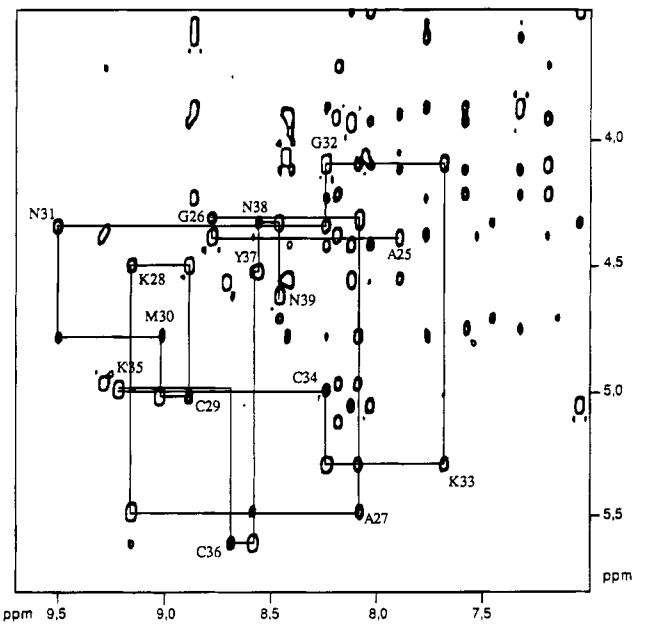

FIGURE 3: NOESY spectrum of NTX (600 MHz, 150 ms mixing time) recorded in H_2O at pH 3.5 and 20 °C. The labels indicate the position of the NH/Hα cross peaks. The sequential $d_{\alpha N}$ connectivities are shown for the β-sheet from residues 25 to 39. Assignment of Lys35 Hα has been determined from the TOCSY and NOESY in D_2O.

two prolines (Pro10 and Pro16) induce breaks in the sequential assignment, but the presence of numerous starting points enabled us to easily overcome this difficulty and to complete the total assignment of the NTX (see chemical shift table in supporting information). The assignment of Pro10 was done using the connectivities between Ser9 Hα and the Hδ protons of Pro10. Assignment of Pro16 was obtained through an NOE between Pro16 Hα and Cys17 NH.

The NMR data confirmed the amidation of the C-terminal residue, which was previously proven on the basis of chemical studies (Nutt et al., 1992). The TOCSY spectra indicate the existence of two extra cross peaks in the amide region. The two TOCSY-correlated protons (7.51 and 7.22 ppm) are connected, through NOESY experiments, to the Hα proton of the last residue (Asn39). This differentiates them from the amide protons of the side chain, which are connected to the Hβ protons in the NOESY spectra, and allowed unambiguous assignment.

Secondary Structure. The secondary structure pattern can be determined directly from NMR data (short-range NOEs, $^3J_{NH-H\alpha}$, and amide−proton exchange experiments) (Figure 2). These data indicate the presence of a helix running from Gln12 to Gly22 (NOE connectivity analysis) or from Pro10 to Leu20 (J-coupling analysis) and a double-stranded antiparallel β-sheet from Ala25 to Asn38. Compared to the canonical α-helix and β-sheet, the following discrepancies are noted: (i) the high value of $^3J_{NH-H\alpha}$ for Cys13 yields a ϕ angle value around 120°, indicating that the helix should be somewhat distorted; (ii) some interstrand correlations are lacking in the β-sheet. The chemical shift index method (Wishart et al., 1992) confirms the existence of the two pieces of secondary structural elements and suggests an extended conformation in the N-terminal extremity, which could form an additional strand in the β-sheet (Figure 2).

Quality of the 3D Structure. Table 1 contains all structural statistics over the 39 final structures calculated from 572

Table 1: Structural Statistics[a,b]

$\langle E(\text{total})\rangle$	$= 297 \pm 7$ kcal·mol^{-1}
$\langle E(\text{bond})\rangle$	$= 32 \pm 1$ kcal·mol^{-1}
$\langle E(\text{angle})\rangle$	$= 115 \pm 4$ kcal·mol^{-1}
$\langle E(\text{dihe})\rangle$	$= 172 \pm 4$ kcal·mol^{-1}
$\langle E(\text{improper})\rangle$	$= 3 \pm 0.3$ kcal·mol^{-1}
$\langle E(\text{VdW})\rangle$	$= -44 \pm 3.3$ kcal·mol^{-1}
energetic cost of deviations from experimental restraints[c]	
$\langle E(\text{NOE})\rangle$	$= 20 \pm 1$ kcal·mol^{-1}
$\langle E(\text{cdihe})\rangle$	$= 0.1 \pm 0.02$ kcal·mol^{-1}
deviations from idealized geometry	
$\langle \text{rmsd (bond)}\rangle$	$= 0.013$ Å
$\langle \text{rmsd (angle)}\rangle$	$= 2.67°$
$\langle \text{rmsd (improper)}\rangle$	$= 2.19°$

[a] All values are averaged on 39 X-PLOR structures. [b] The force field used is parallh22x.pro. The van der Waals energy is calculated with a switched Leonard-Jones potential. Electrical energy has not been taken into account. [c] The values of square-well NOE and dihedral angle potentials are calculated with force constants of 20 kcal/(mol·Å^2) and 50 kcal/(mol·rad^2), respectively.

distance and 42 angle restraints by the geometry and simulated annealing protocol described in the Materials and Methods section. The calculated structures are consistent with both experimental data and the standard covalent geometry. The structures have no distance violations larger than 0.3 Å and no dihedral violations greater than 5°. Furthermore, the covalent geometry is respected, as shown by the low $\langle$rmsd$\rangle$ values of the bond length (0.013 Å) and the valence angles (2.7°). The van der Waals energy is negative (average value −44 kcal/mol), indicating the absence of inappropriate nonbonded contacts.

Analysis of the Ramachandran plot (supporting information, Figure 1a) shows that the ϕ, ψ angle values are in the allowed region, except for the three glycine residues [Gly22, Gly26, and Gly32 (supporting information, Figure 1b,c)], Ser23 which belongs to a floppy loop at the end of the helix, the additional Ala27, Asn31 which is in the $i+2$ position of a β-turn (described below), and Asn38 which is located at the C-terminal extremity of the toxin.

Backbone Structure Description. All of the calculated structures of NTX have a similar backbone folding. Figure 4a shows the superposition of the backbones of the 39 lowest energy structures, and Figure 4b highlights secondary structure elements of the energy-minimized average structure. The general fold is characterized by a helix linked by two disulfide bridges to a three-stranded β-sheet through the consensus sequence Cys-x-x-x-Cys on the helix and Cys-x-Cys on the β-sheet.

The final structures present a fine consistency as indicated by the low rmsd value. The average rmsd of the backbone atoms (N, Cα, C, O) between calculated structures and the mean structure amounts to 0.75 Å. The backbone structure is well-defined except in the following four regions (supporting information, Figure 2b): the N- and C-terminal extremities (i.e., Thr1 and Asn39), the tight turn (Asn31, Gly32), and, to a smaller extent, the loop located at the bottom of the helix (residues from Tyr21 to Ser24). A recalculation of the rmsd excluding these residues falls to a value of 0.39 Å.

Helix. An analysis of the ϕ, ψ values (Figure 5a,b) indicates the existence of a helix spreading over 11 residues, from Pro10 to Leu20. It begins with a proline, known as a good helix inducer (Chou & Fasman, 1974) and ends with a large loop. The helix segment is well-defined, as demonstrated from the low average rmsd over this segment ($\langle$rmsd$\rangle$ = 0.15 Å for backbone atoms of residues 10−20) (supporting information, Figure 2b). The helix is perturbed by the presence of a proline residue at the center (Pro16). An analysis by P-Curve showed that the helix is bent by 40°. Such a proline-induced bend has already been described (Piela et al., 1987). The helix type is difficult to characterize, given that the ψ angle values vary from −74° to 29° along the helix (Figure 5). Since ψ values are more negative at the end of the helix and more positive at its beginning, the helix has been divided in two parts. In the segment 15−20, a hydrogen bond analysis shows that the amide protons of residues 17−19 are linked by $i,i+4$ hydrogen bonds (Figure 6a). This is in agreement with exchange data, which suggest that all amide protons located at the end of the helix are protected. Therefore, as judged from ϕ, ψ values and hydrogen bonding, the structure of the helix segment from residues 15−20 appears to be close to a canonical α-helix. Conversely, the signals of all amido protons of residues 13−15 have disappeared after the first exchange experiment. The segment from residues 10−14 is characterized by $i,i+3$ hydrogen bonds, suggesting a conformation closer to a 3_{10} helix (Figure 6a). This is confirmed by the existence of two NOEs between protons belonging to i and $i+2$ residues ([Cys13 NH−Lys11 Hα] and [Ser14 NH−Gln12 Hα]). However, the $^3J_{\text{NH-H}\alpha}$ coupling constant of Cys13 (over 9 Hz) corresponds to a ϕ angle value of around 120°, indicating that, if the segment 10−14 approaches a 3_{10} helix, this conformation is highly perturbed around Cys13.

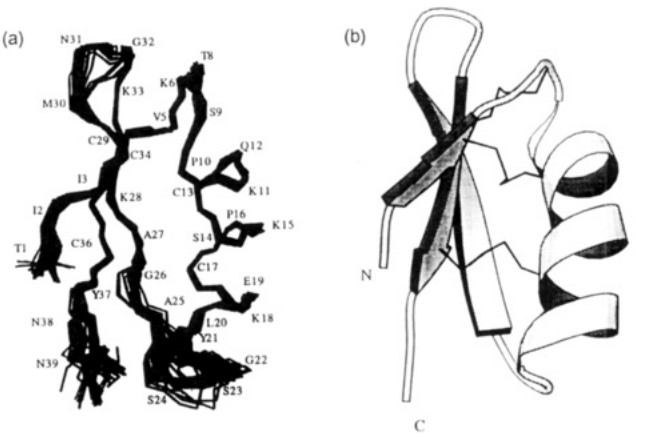

FIGURE 4: (a) Superposition of the backbone atoms of the 39 lowest energy structures of NTX. The view is perpendicular to the helix axis, in order to highlight the bend. (b) Schematic representation of the energy-minimized average structure of NTX, showing the helix, the three-stranded β-sheet, and the disulfide arrangement (thin line). N and C indicate the N- and C-terminal residues respectively. The picture was generated with the MOLSCRIPT program (Kraulis, 1991).

β-Sheet. As implied from the ϕ, ψ values (Figure 5a,b), the β-sheet of NTX is constituted of three strands, including residues 2−3 (β1), residues 25−30 (β2), and residues 33−38 (β3) (Figure 6a). The β-sheet is well-defined (backbone rmsd value = 0.61 Å) (supporting information, Figure 2b). In the average minimized structure, five hydrogen bonds link the two main strands, and two hydrogen bonds connect β1 to β3. Among these bonds, three were introduced as restraints as they displayed slow exchange kinetics (Lys28 NH, Lys33 NH, and Lys35 NH). In fact, regarding the two main strands, all possible hydrogen bonds are observed except between Gly26 O and Tyr37 NH. This is due to the

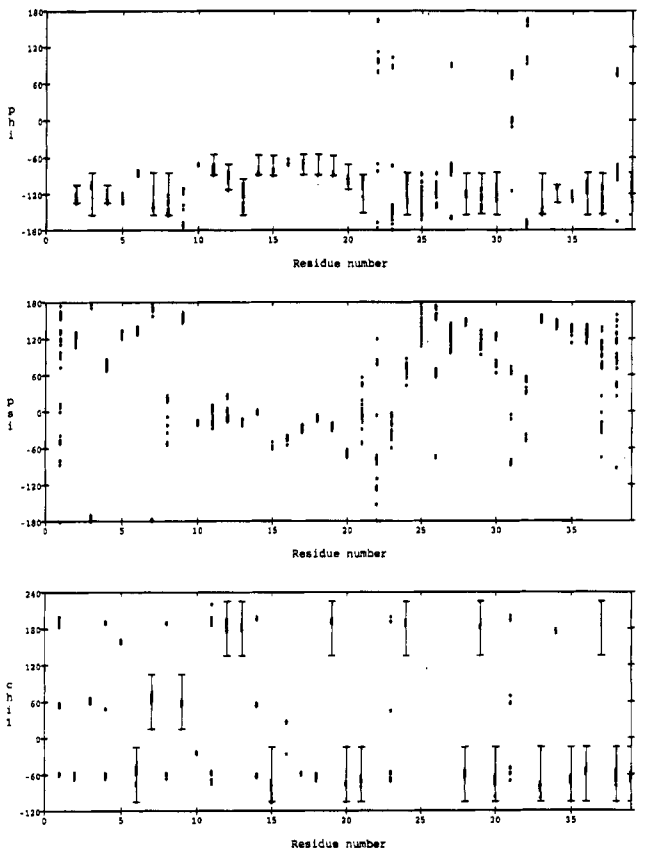

FIGURE 5: ϕ, ψ, and χ_1 angles for each residue in the 39 refined solution structures of NTX. The dihedral restraints applied on ϕ and χ_1 are indicated by vertical bars.

peculiar position of the peptidic plane between Gly26 and Ala27, which is nearly perpendicular to the plane of the β-sheet in the average minimized structure. It can be noted that the $^3J_{NH-H\alpha}$ coupling constant value of Ala27 (7.8 Hz) is abnormally low for a residue lying in a β-sheet. As this value stands in the ambiguous part of the Karplus curve, it does not yield any dihedral restraints. Consistent with the measured value of $J_{NH-H\alpha}$, the Ala27 ϕ angle shows broad variations in the calculated structures (Figure 5a). The presence of the bulkier Ala27 seems to induce some distortion in the β-sheet.

Further analysis of the Ala27 ϕ angle variation reveals three families of structures, according to the values adopted by this angle (Figure 5a). For each group of Ala27 ϕ angles, there is a corresponding group of Gly26 ψ angles (Table 2), yielding three different orientations of the 26−27 peptidic plane. In the first family of structures, the 26−27 peptidic plane has rotated, the Gly26 O pointing toward the helix. The L-α proton of Gly26 points to the side chains of Tyr37 and Asn39, so that the replacement of the glycine by any other amino acid would involve a movement of these two side chains. In the second conformation, the major one (62%), the carboxyl oxygen of Gly26 is facing the solvent while the amide proton of Ala27 points to the helix. The peptidic plane is therefore nearly perpendicular to the plane of the β-sheet, and the two α-protons of Gly26 are facing the solvent. In the third family, the peptidic plane is reversed with the amide proton of Ala27 pointing toward the β3 strand. The two α-protons of Gly26 are facing the solvent. The methyl of Ala27 adopts two different positions, since family 1 and family 3 yield the same location for this side chain. These two positions are close to each other as shown by the low value of the rmsd of this side chain calculated for all 39 structures (0.35 Å). The three families thus established are not energetically distinguishable (Table 2), so a conformational equilibrium may occur between these structures. Finally, the structure of NTX around the additional Ala27 is characterized by a fixed location of the Ala27 and a rotational capacity for the Gly26−Ala27 peptidic plane.

Turn. The two main strands of the β-sheet (25−30, 33−38) are linked to each other by a β-turn, formed by Met30, Asn31, Gly32, and Lys33. This turn appears as a very flexible area as exhibited by the high ⟨rmsd⟩ values of the backbone atoms of Asn31 (i+1 position) which reaches 1.1 Å (supporting information, Figure 2b). A NOE connectivity can be observed between the two amide protons of residues i+1 and i+2, consistent with a type I or I′ turn. But the intensity of this NOE is weak and indicates a 4 Å distance between the two protons. This distance should be far lower (2.6 Å) in a canonical I or I′ turn (Wüthrich, 1986), and then, this NOE does not restrain the structure to this type of turn. A ϕ, ψ angle analysis (Figure 5a,b and supporting information, Figure 1 and Table 2) points out that only a few of the calculated structures are compatible with a type I′ turn conformation (ϕ_2, ψ_2 = 60°, 30° and ϕ_3, ψ_3 = 90°, 0°).

Disulfide Bridges. The pairing of the three disulfide bridges was identified on the basis of conventional experiments based on cleavage of the native NTX with a Lys-c endopeptidase. Three major fractions were resolved by HPLC (not shown) and submitted for microsequencing. The fractions indicated the following amino acid sequences: (1) Pro-Cys-Lys and Cys-Tyr-Asn-Asn, (2) Gln-Cys-Ser-Lys-Pro-Cys-Lys, Cys-Lys, and Cys-Tyr-Asn-Asn, and (3) Cys-Thr-Ser-Pro and Cys-Met-Asn-Gly. Therefore, comparison of these amino acid sequences with that of NTX (Figure 2) unambiguously indicates the following pairing: Cys17−Cys36, Cys13−Cys34, and Cys7−Cys29. It corresponds to the usual pairing of short-chain scorpion toxins possessing the above-mentioned consensus sequence. Two of the three disulfide bridges connect the helix to the third strand of the β-sheet. The third disulfide links the second β-sheet strand to the extended stretch. The conformations of the disulfide are characterized by the dihedral angles reported in Table 3. The two disulfide bridges connecting the helix and the β-sheet are well-defined as evidenced by the low value of their side-chain rmsd (less than 0.3 Å) (supporting information, Figure 3a), yielding a single disulfide conformation in both cases. For the 17−36 disulfide, this conformation is close to the left-handed one, the most common conformation in proteins (Richardson, 1981). The last disulfide is more flexible, and two different conformations can be adopted. The rmsd values of the side chains of the two half-cystines are higher, and that of Cys29 reaches 1.9 Å.

Side Chains. The face of the β-sheet exposed to the solvent can be divided into two parts. The upper part, located at the hairpin extremity, includes three basic lysines (Lys28, Lys33, and Lys35) while only no-charged residues can be observed in the lower part. The opposite face of the β-sheet comprises cysteines (Cys29, Cys34, Cys36) and the hydrophobic residues Ile3, Ala25, and Ala27 (Figure 6b). All these residues belong to the hydrophobic core of the protein, which can be evidenced from the long-range NOEs (see supporting information, Figure 4). This core is composed of the six

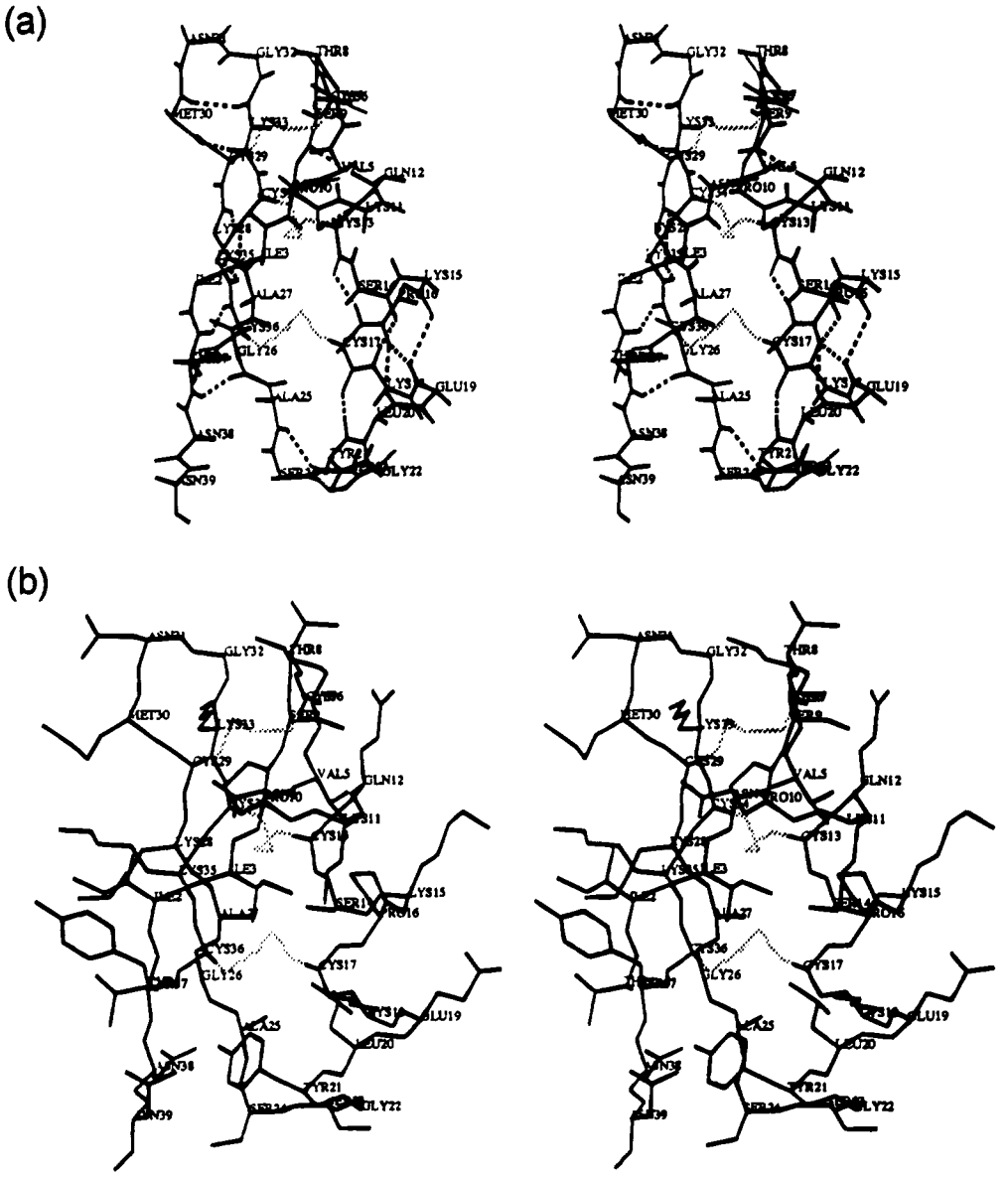

FIGURE 6: (a) Stereoview of the backbone energy-minimized average structure of NTX. The dashed line indicates hydrogen bonds. (b) Stereoview of all non-hydrogen atoms. In both views, the disulfide bridges are shown by gray lines.

Table 2: Characteristics of the Gly26 ψ and Ala27 ϕ Angles in the Three Families of Peptidic Planes

			ϕ, ψ angles (±rmsd)		
family	no. of structures	%	Gly26 ψ	Ala27 ϕ	average energy
all structures	39	100			
family 1	11	28	165 ± 7	-159 ± 1	299 ± 6
family 2	24	62	65 ± 3	-74 ± 5	297 ± 7
family 3	4	10	-74 ± 1	91 ± 2	293 ± 8

cysteines, Ile3, Val5, Ala25, and Ala27, located in the inner face of the β-sheet, and Gln12, Ser14, Pro16, and Leu20 in the helix. All side chains of these residues are characterized by a low relative surface accessibility [rSA lower than 0.45 for all side chains (supporting information, Figure 3b)]. Residues of the core are well-defined (side-chain rmsd < 0.4 Å) except for Cys7 (0.49 Å), Gln12 (1.4 Å), Ser14 (1.15 Å), and Cys29 (1.94 Å) (supporting information, Figure 3a). Remarkably, these four loose residues are close to each other. The core of the toxin comprises therefore a rigid part, composed of the interface between the helix and the β-sheet, and a flexible region, which includes the multiconformation disulfide Cys7−Cys29, and is located near the turn. It should be noted that the interface between the β-sheet and the helix is characterized, for the β1 and β2 strands, by many hydrophobic van der Waals contacts, while the interface between β3 and the helix is achieved by two disulfide bridges (Cys13−Cys34 and Cys17−Cys36).

Regarding residues of the helix, the striking feature is that the side chains of three charged residues, Lys11, Lys15, and Glu19, are pointing out into the solvent (Figure 6b) as shown by their high rSA values (0.82 ± 0.07, 0.69 ± 0.06, and 0.90 ± 0.04, respectively). Nevertheless, the rmsd of two of these side chains remain unusually low for residues that are exposed to the solvent (0.75 and 0.74 Å for Lys15 and Glu19, respectively) (supporting information, Figure 3b), indicating that the two side chains are precisely positioned in the toxin. This may come from the two NOE connectivities existing between the Hγ protons of the side chains of both Lys15 and Glu19 with Pro16, a precisely defined residue (rmsd = 0.23 Å). The location of the Lys11 side chain is more diffuse (side-chain rmsd = 1.12 Å).

Table 3: Conformation of the Three Disulfide Bridges in the 39 Solution Structures of NTX

S−S bridges	no. of structures	%	χ angles (±rmsd)				
			$\langle\chi^1_i\rangle$	$\langle\chi^2_i\rangle$	$\langle\chi^3$ss$\rangle$	$\langle\chi^2_j\rangle$	$\langle\chi^1_j\rangle$
Cys7−Cys29 (family 1)	27	69	62.6 ± 2.0	90.4 ± 1.7	107.3 ± 1.4	70.9 ± 3.4	−175.9 ± 0.9
Cys7−Cys29 (family 2)	31	31	72.3 ± 1.9	−162.2 ± 2.2	−120.5 ± 1.4	−115.3 ± 3.4	−134.9 ± 0.2
Cys13−Cys34	39	100	−177.8 ± 2.6	45.3 ± 1.9	85.9 ± 1.6	44.8 ± 1.9	175.9 ± 1.4
Cys17−Cys36	39	100	−57.3 ± 0.9	−62.4 ± 7.8	−78.5 ± 1.7	−48.3 ± 3.0	−55.3 ± 1.9

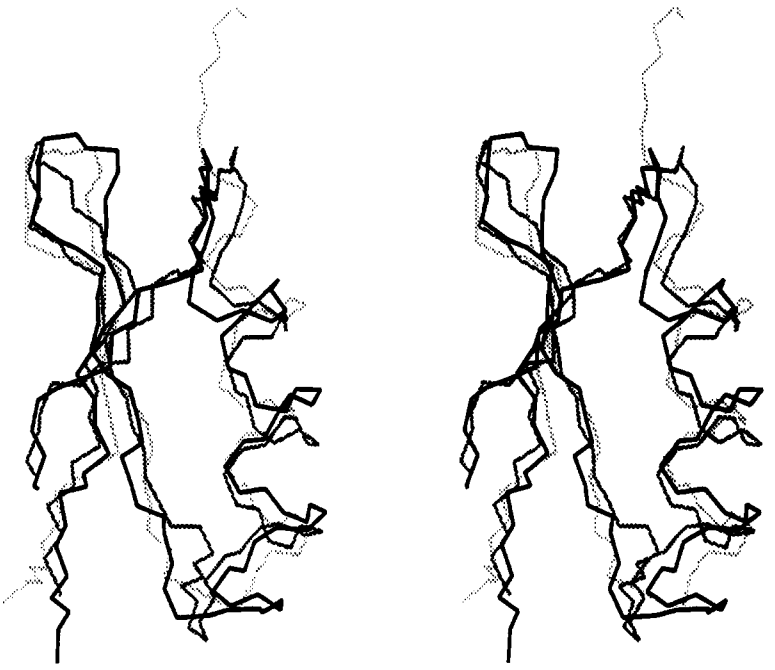

FIGURE 7: Stereoview of NTX (bold line), ChTX (dark gray line), and PO5-NH_2 (light gray line) structures, where the helix and the two-stranded β-sheet backbone of the three toxins were superimposed. The NTX structure is the mean minimized structure. ChTX and PO5-NH_2 structures are the number 1 referenced structure in PDB.

DISCUSSION

We have shown that NTX adopts an α/β fold that is primarily composed of a three-stranded β-sheet, ensuring intimate contacts with a short helical fragment. This fold is commonly shared by several other proteins (Bontems et al., 1991) which include (i) other toxins of similar size and that act on K^+ channels or Cl^- channels (Bontems et al., 1992; Johnson & Sugg, 1992; Meunier et al., 1993; Fernandez et al., 1994; Johnson et al., 1994; Lippens et al., 1995), (ii) scorpion toxins that possess a longer polypeptide chain (60−70 amino acids) and which act on Na^+ channels (Fontecilla-Camps et al., 1988; Darbon et al., 1991; Zhao et al., 1992), (iii) insect defensins (Hanzawa et al., 1990; Bonmatin et al., 1992), and (iv) thionins from plants (Bruix et al., 1993). Clearly, the α/β fold exerts a remarkable functional diversity; however, the detailed structure−activity relationships that are associated with it remain poorly understood.

In this respect, it is well-known that scorpions produce a variety of toxins acting on K^+ channels, but which differ from each other by a wide diversity of specificities. We proceeded, therefore, to a detailed comparison of the 3D structure of NTX with those of ChTX (37 amino acids), PO5-NH_2 (31 amino acids), and KTX (37 amino acids), which display differential selectivities toward K^+ channels and for which the structural coordinates are available in the Protein Data Bank. The structure of NTX appears to be rather close to those of ChTX (Bontems et al., 1992) and PO5-NH_2 (Meunier et al., 1993), with respective backbone rmsd values equal to 1.33 ± 0.1 and 1.52 ± 0.1 Å (Figure 7). A larger difference is observed with KTX with an rmsd equal to 6.39 ± 0.1 Å. This difference is accounted for by a different position adopted by the N-terminal extremity in KTX, as already mentioned (Fernandez et al., 1994). Despite the low rmsd values observed with ChTX and PO5-NH_2, the relative positions of the helix and the β-sheet vary in these toxins. This variation can be geometrically characterized by the angle between the helix and the β3-strand axis, which was estimated by P-Curve to be 13° in PO5-NH_2, 50° in ChTX, and 32° in NTX (see Materials and Methods). For MgTX, another toxin whose 3D structure was recently described, this angle was evaluated to be 40° (Johnson et al., 1994). The sharper angle in PO5-NH_2 may be related to the shorter length of the fragment that links Cys3 and Cys8. Indeed, four residues separate the first two cysteines in PO5-NH_2, instead of five in the other toxins. This shorter fragment might force the helix at the N-terminal extremity to be closer to the hairpin.

A detailed examination of toxin structures reveals further differences in the secondary structural elements that constitute their common α/β motif. First, the lengths of the β-sheets and helices are variable. The β-sheet is longer (six residues) in NTX and MgTX (Johnson et al., 1994) than in other compared toxins, where it includes only five residues. This longer length is due to two additional amino acids in these two toxins which both have 39 residues (Figure 1). The helix of NTX spans 11 residues, from Pro10 to Leu20,

appearing longer than in other toxins, where the helix length varies, according to the authors, from 7 in KTX to 10 in ChTX, MgTX, and IbTX. Second, prolines are included in the helices of three of these related toxins. Thus, KTX and NTX have two prolines in the helix and MgTX has three prolines. One of them, Pro10, is always located at the N-terminal extremity of the helix. The other proline (Pro16) is located in the middle of the helix (Figure 1), providing a local structural dichotomy in both NTX and KTX. Thus, in NTX, the helix begins with a 3_{10} helix, whereas it ends with a clear α-helical conformation. Conversely, in KTX, the helix begins with an α-helix and ends with a 3_{10} helix. No such structural effects were found in MgTX, which has two prolines in the middle of its helix. Nevertheless, the helix of MgTX is somewhat disrupted, as indicated by the high value for its Cys 13 $^3J_{NH-H\alpha}$ coupling constant (Johnson et al., 1994).

Another interesting feature of the scaffold lies in the bending capacity of its helix. NTX displays a high degree of curvature, since calculation with P-Curve (see Materials and Methods) indicated a 40° angle (Figure 4). Examination of the previously published structures of other scorpion toxins revealed that KTX also has a helix with a high degree of curvature (62°), whereas the helices of ChTX and PO5-NH_2 undergo a weaker bending, with 16° and 8° angles, respectively. This sharp bending observed in both NTX and KTX could be commonly associated with the presence of a proline at position 16 (Figure 1) which, as discussed above, disrupts the regular organization of the helix. Nevertheless, in NTX, this bend may have another structural role. It was previously noted that the space that exists within the contact area between the helix and the β-sheet of ChTX is so limited that it can only accommodate a proton (Bontems et al., 1991). As a result, in most toxins, this position is conveniently occupied by a glycine which was proposed to be part of the consensus pattern of scorpion toxins, within the pattern Gly_{26}-x-Cys_{28} (Ménez et al., 1992). In contrast, in NTX, the corresponding position is occupied by the bulkier methyl side chain of an alanine residue (Ala27). We wish to suggest that the high degree of curvature of the helix nicely allows the accommodation of Ala27.

NTX was the first inhibitor of K^+ channels isolated from scorpion venoms (Carbone et al., 1982). Since then, studies have largely concentrated on its pharmacological properties (Carbone et al., 1982, 1987; Sitges et al., 1986); however, the molecular elements that are associated with its specificity remain to be established. It was shown that NTX has a strong binding affinity for $K_{v1,3}$, whereas it exerts a weaker affinity for the Ca^{2+}-activated K^+ channels (BK). This is in contrast to ChTX, which displays a much higher affinity for BK than for $K_{v1,3}$. The binding of ChTX to BK was studied by mutational analysis, which demonstrated the importance of eight residues (Ser10, Trp14, Arg25, Lys27, Met29, Asn30, Arg34, and Tyr36) (Stampe et al., 1994). Five of these eight residues (Lys27, Met29, Asn30, Arg34, and Tyr36) were shown to be critical for the recognition of a voltage-dependent K^+ channel (Shaker) by ChTX (Goldstein et al., 1994). Examination of the amino acid sequences of both ChTX and NTX clearly reveals that these five residues are present in both toxins [with a conservative mutation Arg34 (ChTX) into Lys35 (NTX)], while the three other residues, which are crucial for binding of ChTX to BK, are lacking in NTX. Two of these three residues are located in the helix (Ser10 and Trp14), and the third one, Arg25, is at the base of the β-sheet. Therefore, a homogeneous portion of the functional surface of ChTX is lacking in NTX, thus offering a possible explanation for its weak affinity for BK. The five common residues probably assure the residual binding affinity of NTX for this channel. A related question remains as to which residues provide NTX with its high affinity for $K_{v1,3}$. Previous studies done with hybrid toxins composed of portions of ChTX and IbTX (Giangiacomo et al., 1993) argue for the importance of the β-sheet in ChTX for recognition of $K_{v1,3}$. As the five residues crucial for ChTX binding to the Shaker are found in the β-sheet and conserved in NTX and MgTX, two toxins with a high affinity for $K_{v1,3}$, these residues may be implicated in the binding to both types of voltage-dependent K^+ channels, $K_{v1,3}$ and Shaker. Strikingly, in IbTX, a toxin which does not bind $K_{v1,3}$, only one of these residues is mutated (Asn30Gly). An Asn30Gly mutant was synthesized while investigating the residues involved in the molecular recognition between ChTX and the Shaker channel and showed the highest drop in affinity among all mutations tested (Goldstein et al., 1994). Therefore, Asn30 (ChTX numbering) appears important for the two types of voltage-dependent channels, and actually, this residue can be observed in all the short-chain scorpion toxins which bind $K_{v1,3}$ (NTX, MgTX, ChTX, KTX, and $AgTX_{1,2,3}$). Moreover, the structural study reported in this paper emphasizes the flexibility of Asn31 (NTX numbering), which is located in the $i+1$ position of the β-turn and which has the highest side-chain rmsd (5.5 Å) in NTX, much greater than all other side chains (supporting information, Figure 2b).

The K^+ channels were shown to have negatively charged residues near their pore (Anderson et al., 1988), and it was proposed that these ionized carboxyl groups are involved in ion conduction (MacKinnon et al., 1989; MacKinnon & Miller, 1989). These charges also take part in the binding of cationic pore blockers by establishing a local negative potential at the pore entrance (Anderson et al., 1988; MacKinnon et al., 1989). As short-chain scorpion toxins are basic proteins, they are expected to establish electrostatic interactions with the K^+ channels, and actually, three positively charged residues of ChTX are functionally important residues (Stampe et al., 1994). We proposed above that two of these, Lys28 and Lys35, may also be involved in the interaction of NTX to $K_{v1,3}$. With the view to get a better insight into the distribution of electrostatic charges at the surface of NTX, we submitted its 3D structure to DELPHI (Gilson & Honig, 1988) and compared it with the electrostatic distribution at the ChTX surface (Figure 8). For both toxins, calculations of the electrostatic potential on the Connolly surfaces (solvent-accessible surface) yield (i) a confined surface with a negative value in one-half of the helix and (ii) a high positive value on a large surface of the β-sheet and on the other half of the helix. Nevertheless, some variations occur within these two general features: (i) the location of the Connolly surface with a negative value, largely due to the glutamate residue, differs in the two toxins; (ii) in the helix of NTX, a group of three spatially adjacent lysines (Lys11, Lys15, and Lys18) forms an arc of a circle around the Ser14 side chain and constitutes a high density of positive charges, while in ChTX, due to the absence of Lys15, such a high electrostatic potential is not observed on the surface of the helix.

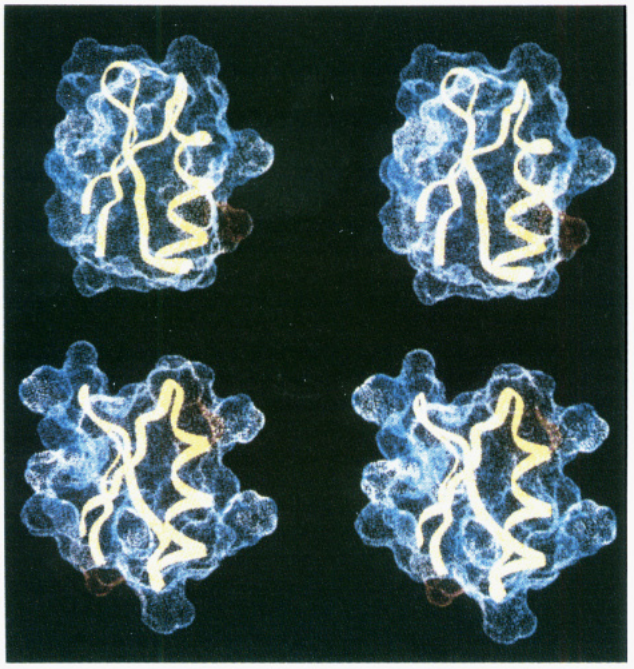

FIGURE 8: Stereoview of electrostatic surfaces of NTX (top) and ChTX (bottom) as calculated by the program DELPHI. Positively and negatively charged residues are displayed in white and red, respectively.

A common consensus sequence, Cys-[...]-Cys-x-x-x-Cys-[...]-Gly-x-Cys-[...]-Cys-x-Cys, was previously claimed to reflect the presence in a protein of the α/β scaffold that has been analyzed in this paper. Our comparative study between the 3D structure of NTX and the available 3D structures of other short-chain scorpion toxins highlights the structural plasticity of this scaffold. In particular, the helix bends with varying degrees of curvature, and different relative orientations are adopted by the helix and β-sheet. Presumably, this plasticity concurs to the accommodation of a variety of changes that occur within the consensus sequence, such as the insertion of an additional residue in the Gly-x-Cys pattern.

ACKNOWLEDGMENT

We thank Dr. S. Furois for help using P-Curve software, Dr. N. Julian of Biosym Technologies Co. for providing and helping using DELPHI, Dr. I. Segalas for her overall kindness while showing the use of modeling softwares, and Drs. L. Remerowski and S. Zinn-Justin for their fruitful comments during the writing of this paper. The DIANA program was provided by Prof. K. Wüthrich and the X-PLOR program by Dr. A. Brünger.

SUPPORTING INFORMATION AVAILABLE

Table 1 showing chemical shifts of protons at 20 °C, Table 2 giving an analysis of ϕ, ψ angle values for the two residues, Asn31 and Gly32, of the β-turn, Figure 1 showing Ramachandran plots, Figure 2 showing the number of NOEs (intra, sequential, long-range) per residue along the sequence (a) and the rmsd of backbone heavy atoms (b), Figure 3 showing the rmsd of side-chain heavy atoms (a) and surface accessibility of side chains (b), and Figure 4 showing a diagonal plot of the connectivities between residues along the sequence (9 pages). Ordering information is given on any current masthead page.

REFERENCES

Anderson, C., MacKinnon, R., Smith, C., & Miller, C. (1988) *J. Gen. Physiol. 91*, 317−333.
Aue, W. P., Bartholdi, E., & Ernst, R. R. (1976) *J. Chem. Phys. 64*, 2229−2246.
Baker, E. N., & Hubbard, R. E. (1984) *Prog. Biophys. Mol. Biol. 44*, 97−179.
Bonmatin, J. M., Bonnat, J. L., Gallet, X., Vovelle, F., Ptak, M., Reichart, J. M., Hoffman, J. A., Keppi, E., Legrain, M., & Achstetter, T. (1992) *J. Biomol. NMR 2*, 235−256.
Bontems, F., Roumestand, C., Gilquin, B., Ménez, A., & Toma, F. (1991) *Science 254*, 1521−1523.
Bontems, F., Gilquin, B., Roumestand, C., Ménez, A., & Toma, F. (1992) *Biochemistry 31*, 7756−7764.
Braunschweiler, L., & Ernst, R. R. (1983) *J. Magn. Reson. 53*, 521−528.
Bruix, M., Jiménez, M. A., Santoro, J., Gonzalez, C., Colilla, F. J., Méndez, E., & Rico, M. (1993) *Biochemistry 32*, 715−724.
Brünger, A. T. (1992) *X-PLOR Version 3.1: A System for X-Ray Crystallography and NMR*, Yale University Press, New Haven and London.
Brünger, A. T., Kuriyan, K., & Karplus, M. (1987) *Science 235*, 458−460.
Carbone E., Wanke, E., Prestipino, G., Possani, L. D., & Maelicke, A. (1982) *Nature 296*, 90−91.
Carbone, E., Prestipino, G., Spadavecchia, L., Franciolini, F., & Possani, L. D. (1987) *Pfluegers Arch. 408*, 423−431.
Chou, P. Y., & Fasman, G. D. (1974) *Biochemistry 13*, 211−222.
Darbon, H., Weber, C., & Braun, W. (1991) *Biochemistry 30*, 1836−1845.
Davis, D. G., & Bax, A. (1985) *J. Am. Chem. Soc. 107*, 2820−2821.
Fernandez, I., Romi, R., Szendeffy, S., Martin-Eauclaire, M. F., Rochat, H., Van Rietschoten, J., Pons, M., & Giralt, E. (1994) *Biochemistry 33*, 14256−14263.
Fontecilla-Camps, J., Habersetzer-Rochat, C., & Rochat, H. (1988) *Proc. Natl. Acad. Sci. U.S.A. 85*, 7443−7447.
Furois-Corbin, S., Smith, J. C., & Lavery, R. (1994) *Biopolymers 35*, 555−571.
Garcia-Calvo, M., Leonard, R. J., Novick, J., Stevens, S. P., Scmalhofer, W., Kaczorowski, G. J., & Garcia, M. L. (1993) *J. Biol. Chem. 268*, 18866−18874.
Giangiacomo, K. M., Garcia, M. L., & McManus, O. B. (1992) *Biochemistry 31*, 6719−6727.
Giangiacomo, K. M., Sugg, E. E., Garcia-Calvo, M., Leonard, R. J., McManus, O. B., Kaczorowski, G. J., & Garcia, M. L. (1993) *Biochemistry 32*, 2363−2370.
Gilquin, B., Roumestand, C., Zinn-Justin, Ménez, A., & Toma, F. (1993) *Biopolymers 33*, 1659−1675.
Gilson, M., & Honig, B. (1988) *Proteins 4*, 7−18.
Gippert, G. P., Yip, P. F., Wright, P. E., & Case, D. A. (1990) *Biochem. Pharmacol. 40*, 15−22.
Goldstein, S. A. N., & Miller, C. (1993) *Biophys. J. 65*, 1613−1619.
Goldstein, S. A. N., Pheasant, D. J., & Miller, C. (1994) *Neuron 12*, 1377−1388.
Güntert, P., Braun, W., & Wüthrich, K. (1991) *J. Mol. Biol. 217*, 517−530.
Gurolla, G. B., Molinar-Rode, R., Sitges, M., Bayon, A., & Possani, L. D. (1989) *J. Neural. Transm. 77*, 11−20.
Hanzawa, H., Shimada, I., Kuzuhara, T., Komano, H., Kohda, D., Inagaki, F., Natori, S., & Arata, Y. (1990) *FEBS Lett. 269*, 413−420.
Hyberts, S. G., Märki, W., & Wagner, G. (1987) *Eur. J. Biochem. 164*, 625−635.
Johnson, B. A., & Sugg, E. E. (1992) *Biochemistry 31*, 8151−8159.
Johnson, B. A., Stevens, S. P., & Williamson, J. M. (1994) *Biochemistry 33*, 15061−15070.
Karplus, M. (1963) *J. Am. Chem. Soc. 85*, 2870−2871.
Koppenhörfer, E., & Schmidt, H. (1968) *Pfluegers Arch. 303*, 133−149.
Kraulis, P. (1991) *J. Appl. Crystallogr. 24*, 946−950.

Kumar, A., Ernst, R. R., & Wüthrich, K. (1980) *Biochem. Biophys. Res. Commun. 95*, 1−6.
Lee, B., & Richards, F. M. (1971) *J. Mol. Biol. 55*, 379−400.
Leonard, R. J., Garcia, M. L, Slaughter, R. S., & Reuben, J. P. (1992) *Proc. Natl. Acad. Sci. U.S.A. 89*, 10094−10098.
Lippens, G., Najib, J., Wodak, S. J., & Tartar, A. (1995) *Biochemistry 34*, 13−21.
MacKinnon, R., & Miller, C. (1989) *Biochemistry 28*, 8087−8092.
MacKinnon, R., Latorre, R., & Miller, C. (1989) *Biochemistry 28*, 8092−8099.
Menez, A., Bontems, F., Roumestand, C., Gilquin, B., & Toma, F. (1992) *Proc. R. Soc. Edinburgh 99B*, 83−103.
Meunier, S., Bernassau, J. M., Sabatier, J. M., Martin-Eauclaire, M. F., Van Rietschoten, J., Cambillau, C., & Darbon, H. (1993) *Biochemistry 32*, 11969−11976.
Miller, C., Moczydlowski, E., Latorre, R., & Phillips, M. (1985) *Nature 313*, 316−318.
Miller, S., Janin, J., Lesk, A. M., & Chothia, C. (1987) *J. Mol. Biol. 196*, 641−656.
Narahashi, T., Shjapiro, D. I., Geduchi, T., Scuka, M., & Wang, C. M. (1972) *Am. J. Physiol. 222*, 850−857.
Nilges, M., Gronenborn, A. M., Brünger, A. T., & Clore, G. M. (1988) *Protein Eng. 2*, 27−38.
Nutt, F. N., Arison, B. H., & Smith, J. S. (1992) *Peptides*, 101−102.
Pardi, A., Billeter, M., & Wüthrich, K. (1984) *J. Mol. Biol. 180*, 741−751.
Park, C. S., & Miller, C. (1992) *Neuron 9*, 307−313.
Piela, L., Nemethy, G., & Scheraga, H. A. (1987) *Biopolymers 26*, 1587−1600.
Possani, L. D., Martin, B. M., & Svendsen, I. (1982) *Carlsberg Res. Commun. 47*, 285−289.
Rance, M. (1987) *J. Magn. Reson. 74*, 557−564.
Rance, M., Sorensen, O., Bodenhausen, G., Wagner, G., Ernst, R. R., & Wüthrich, K. (1983) *Biochem. Biophys. Res. Commun. 117*, 479−485.
Richardson, J. (1981) *Adv. Protein Chem. 34*, 267−330.
Romey, G., Chicheportiche, R., Lazdunski, M., Rochat, H., Miranda, F., & Lissitzky, S. (1975) *Biochem. Biophys. Res. Commun. 64*, 115−121.
Sands, S. B., Lewis, R. S., & Cahalan, M. D. (1989) *J. Gen. Physiol. 93*, 1061−1074.
Segalas, I., Roumestand, C., Zinn-Justin, Gilquin, B., Ménez, R., Ménez, A., & Toma, F. (1995) *Biochemistry 34*, 1248−1260.
Shaka, A. J., Keeler, J., & Freeman, R. (1983) *J. Magn. Reson. 53*, 313−334.
Sitges, M., Possani, L. D., & Bayon, A. (1986) *J. Neurosci. 6*, 1570−1574.
Sklenar, H., Etchebest, C., & Lavery, R. (1989) *Proteins 6*, 46−60.
Stampe, P., Kolmakova-Partensky, L., & Miller, C. (1994) *Biochemistry 33*, 443−450.
States, D. J., Haberkorn, R. H., & Ruben, D. J. (1986) *J. Magn. Reson. 48*, 286−292.
Swanson, R., Marshall, J., Smith, J. S., Williams, J. B., Boyle, M. B., Folander, K., Luneau, C. J., Antanavarge, J., Olivia, C., Buhrow, S. A., Bernett, C., Stein, R. B., & Kaczmarek, L. K. (1990) *Neuron 4*, 929−939.
Vaca, L., Gurrola, G. B., Possani, L. D., & Kunze, D. L. (1993) *J. Membr. Biol. 134*, 123−129.
Valdivia, H. H., Smith, J. S., Martin, B. M., Coronado, R., & Possani, L. D. (1988) *FEBS Lett. 226*, 280−284.
Wilmot, C. M., & Thornton, J. M. (1990) *Protein Eng. 3*, 479−493.
Wishart, D. S., Sykes, B. D., & Richards, F. M. (1992) *Biochemistry 31*, 1647−1651.
Wüthrich, K. (1986) *NMR of Proteins and Nucleic Acids*, Wiley-Interscience, New York.
Zhao, B., Carson, M., Ealick, S. E., & Bugg, C. E. (1992) *J. Mol. Biol. 227*, 239−252.
Zinn-Justin, S., Roumestand, C., Gilquin, B., Bontems, F., Ménez, A., & Toma, F. (1992) *Biochemistry 31*, 11335−11347.

BI951700X